Xiangchun Xuan[1]*
Dongqing Li[2]

[1]Department of Mechanical & Industrial Engineering, University of Toronto, Toronto, Ontario, Canada
[2]Department of Mechanical Engineering, Vanderbilt University, Nashville, TN, USA

Received July 21, 2006
Revised September 15, 2006
Accepted September 15, 2006

Research Article

Solute separation in nanofluidic channels: Pressure-driven or electric field-driven?

We demonstrate theoretically that solute separation can be accomplished in pressure-driven flow through nanochannels due to solute–wall interactions. Such pressure-driven separation is efficient in identifying solutes with variable valences. This function complements exactly the electric field-driven separation (*i.e.*, electrophoretic separation) in nanofluidic channels that works well for solutes differing in diffusivity. We also demonstrate the enhanced separation of solutes of either different valence or different diffusivity through the combination of a pressure-driven flow and an electric field-driven backflow in nanofluidic channels. This combined flow, however, has to be used with caution for solutes varying in both valence and diffusivity.

Keywords:
Electroosmosis / Nanofluidic channel / Pressure-driven flow / Solute separation
DOI 10.1002/elps.200600454

1 Introduction

CE is a routine analytical technique to separate charged solutes differing in electrophoretic mobility in microchannels [1]. As an important alternative to this electric field-driven separation, LC is useful for the separation of solutes varying in interaction with a stationary phase when they are forced by pressure through a microcolumn [2]. Considering the growing demand of integrated nanofluidic systems [3, 4] and the advances in nanochannel fabrication [5–10], it is natural to ask the question whether solute separation can also be realized in nanofluidic channels by pressure- or electric field-driven processes.

Recently, electrophoretic separation of fluorescent dyes was implemented in nanochannels. Garcia *et al.* [11] observed that the nanoconfinement of electrokinetic transport resulted in enhanced electrophoretic separation of negatively charged Alxea dye from neutral rhodamine B dye. Their experimental data of dye velocity agreed well with a proposed concentration-weighted velocity. Pennathur and Santiago [12–15] analyzed the solute electrokinetic transport in nanochannels, and demonstrated the electrokinetic separation of fluorescein and Bodipy by ion valence that they termed EKSIV. More recently, Xuan and Li [16] investigated numerically the influence of transverse electromigration on electrokinetic transport of charged solutes in a series of micro- and nanochannels. They found that this crosswise motion of solutes in response to the electrical double layer (EDL) field, which is often ignored in previous studies, could significantly affect the electrokinetic migration velocity in nanochannels and the electrokinetic dispersion in microchannels.

As it is essentially the consequence of solute–wall interactions, the transverse electromigration of charged solutes within EDL should affect their transport and separation in nanofluidic channels regardless of the flow pattern of the BGE. This article is going to examine the feasibility of solute separation in pressure-driven nanochannel flow and then compare its efficiency with that in electric field-driven nanochannel flow.

Correspondence: Professor Dongqing Li, Department of Mechanical Engineering, Vanderbilt University, 2301 Vanderbilt Place, Nashville, TN 37235-1592, USA
E-mail: dongqing.li@vanderbilt.edu
Fax: +1-615-343-6687

Abbreviation: EDL, electrical double layer

2 Theoretical formulation

2.1 Notation

(see Addendum)

2.2 Solute transport in nanofluidic channels

Given the fact that the width (in micrometers) of state-of-the-art nanofluidic channels is usually much larger than the depth (in nanometers) [5–15], we consider the transport of a solute zone in a slit nanochannel, see Fig. 1 for the schematic. Apparently, two solutes can be separated if their zones migrate at different velocities. This section presents the

* Current address: Department of Mechanical Engineering, Clemson University, Clemson, SC 29634-0921, USA

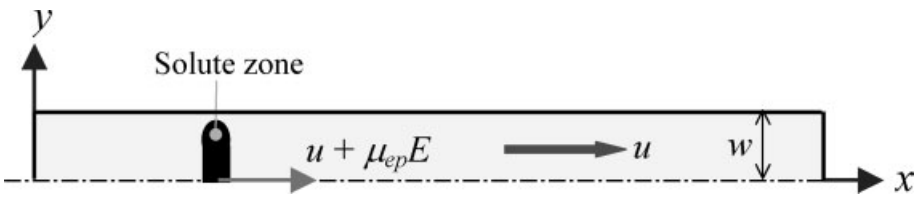

Figure 1. Scheme of the solute transport in a slit nanochannel. The dashed-dotted line indicates the channel axis. For definition of symbols refer to Notation (see Addendum).

derivation of the mean migration velocity of a solute zone. The analysis of solute separation in nanochannels will be provided in the following section.

Assuming a fully developed flow of the BGE (either pressure- or electric field-driven), the electrokinetic transport of solutes in a slit nanochannel is governed by the following 2-D Nernst–Planck equation

$$\frac{\partial c}{\partial t} + \left(u + \mu_{ep}E\right)\frac{\partial c}{\partial x} = D\frac{\partial^2 c}{\partial x^2} + D\frac{\partial^2 c}{\partial y^2} + \mu_{ep}\frac{\partial}{\partial y}\left(c\frac{\partial \psi}{\partial y}\right) \quad (1)$$

where c is the solute concentration, t is the time coordinate, u is the velocity of the BGE in the x-direction, μ_{ep} is the solute electrophoretic mobility (also called ionic mobility), E is the axial electric field either externally applied in EOF or internally induced in pressure-driven flow (*i.e.*, so-called streaming potential field) [17–19], x and y are the longitudinal and transverse coordinates originating from the axis of the channel inlet (see Fig. 1), D is the solute diffusivity, and ψ is the EDL potential that varies only in the y-direction. Integrating Eq. (1) over the channel cross-section drops the terms involving the y-coordinate because of the no-flux boundary condition

$$\frac{\partial \bar{c}}{\partial t} + \frac{\partial \overline{(u + \mu_{ep}E)c}}{\partial x} = D\frac{\partial^2 \bar{c}}{\partial x^2} \quad (2)$$

where the overbar indicates the average over the cross-section. Equation (2) is valid in straight channels of arbitrary cross-sectional shape [20]. However, it provides no direct knowledge of either the mean migration velocity or the effective dispersion coefficient of solutes, where the former determines whether solutes can be separated while the latter governs the resolution [21]. As the hydrodynamic dispersion is proportional to the square of the channel transverse dimension in both pressure- [22, 23] and electric field-driven flows [24, 25], it becomes trivial in nanochannels even though the variation of fluid velocity across the channel may become very significant [6–9, 11–15]. Moreover, such dispersion has no direct influence on the mean migration velocity of solutes. Therefore, we neglect the hydrodynamic dispersion in this article and focus primarily on the migration velocity with regard to solute separation.

Following the analysis of Pennathur and Santiago [12–15], we drop the terms associated with the longitudinal (x-coordinate) concentration gradient (thus neglect the hydrodynamic dispersion). Also a quasi-steady equilibrium of the solutes is assumed in the transverse direction, reducing Eq. (1) to

$$0 = D\frac{\partial^2 c(x,y,t)}{\partial y^2} + \mu_{ep}\frac{\partial}{\partial y}\left(c(x,y,t)\frac{\partial \psi}{\partial y}\right) \quad (3)$$

Invoking the Nernst–Einstein equation [18], $\mu_{ep} = Dz_v e/k_B T$, and integrating Eq. (3) twice gives [7, 12–18]

$$c(x,y,t) = c_c(x,t)\exp\left[-\frac{z_v e}{k_B T}(\psi - \psi_c)\right] \quad (4)$$

where c_c and ψ_c are, respectively, the solute concentration and the EDL potential at the channel axis, z_v is the valence of solutes, e is the charge of a proton, k_B is the Boltzmann's constant, and T isthe liquid temperature. Thus, substituting Eq. (4) into Eq. (2) leads to

$$\frac{\partial c_c}{\partial t} + U_s\frac{\partial c_c}{\partial x} = D\frac{\partial^2 c_c}{\partial x^2} \quad (5)$$

where U_s is the mean migration velocity of a solute zone in nanochannels given by

$$U_s = \overline{u\exp\left(-\frac{z_v e\psi}{k_B T}\right)}\Big/\overline{\exp\left(-\frac{z_v e\psi}{k_B T}\right)} + \mu_{ep}E \quad (6)$$

Apparently the U_s of neutral solutes ($z_v = 0$), $U_{neutral} = \bar{u}$, is only associated with the flow velocity of BGE. For charged solutes, however, the valence z_v also plays an important role in U_s, which underlies the solute separation in pressure-driven nanochannel flows and will be addressed in detail shortly. A closed form solution of c_c is available from Eq. (5), so that the electrokinetic transport of charged solutes in nanochannels is described by [26]

$$c(x,y,t) = \frac{c_0}{2}\left[\mathrm{erf}\left(\frac{w_0 - x + X_0 + U_s t}{2\sqrt{Dt}}\right) + \right.$$
$$\left. + \mathrm{erf}\left(\frac{w_0 + x - X_0 - U_s t}{2\sqrt{Dt}}\right)\right]\exp\left(-\frac{z_v e\psi}{k_B T}\right) \quad (7)$$

where c_0 is the initial solute concentration, erf is the error function, w_0 is the half-width of the initially uniform solute zone, and X_0 is the x-coordinate of the center of the initial solute zone. It is important to note that Eq. (7) is accurate only in very small nanochannels where the effective dispersion coefficient is reduced to diffusion coefficient D [12–15]. In relatively large nanochannels (*e.g.*, submicrometer channels) or if the solute diffusivity is extremely small, however, D should be replaced by the effective dispersion coefficient of either a higher or lower magnitude [18].

The EDL potential ψ and the fluid velocity u in the last two equations are given by (see the Addendum for the derivations)

$$\psi = \zeta \frac{\cosh(\kappa y)}{\cosh(\kappa w)} \tag{8}$$

$$u = \mu_{pd}\left(1 - \frac{y^2}{w^2}\right)P + \mu_{eo}\left(1 - \frac{\psi}{\zeta}\right)E \tag{9}$$

where ζ is the wall zeta potential, w is the half-channel width, $\kappa = \sqrt{2e^2 n_0/\varepsilon k_B T}$ the inverse of Debye length with n_0 the ionic density of the bulk electrolyte, $\mu_{pd} = w^2/2\eta$ the defined pressure-driven mobility (in unit of $ms^{-1}Pa^{-1}$), $\mu_{eo} = -\varepsilon\zeta/\eta$ the electroosmotic mobility (in unit of $m^2s^{-1}V^{-1}$, positive if the zeta potential ζ is assumed negative), η is the liquid viscosity, and P is the pressure drop *per* unit channel length. Note that the so-called Debye–Hückel approximation [17–19] has been utilized to get Eq. (8), which requires essentially a low magnitude of ζ (smaller than 25 mV). However, we have demonstrated recently using numerical simulation the fairly good accuracy of Eq. (8) in predicting the solute migration velocity U_s at $\zeta = -50$ mV [16]. Therefore, U_s in Eq. (6) is specified as

$$U_s = \mu_{pd}P\frac{\overline{\left(1 - \frac{y^2}{w^2}\right)G(\gamma)}}{\overline{G(\gamma)}} + \mu_{eo}E\frac{\overline{\left[1 - \frac{\cosh(\kappa y)}{\cosh(K)}\right]G(\gamma)}}{\overline{G(\gamma)}} + z_v\mu_{ep}^* E \tag{10}$$

$$G(\gamma) = \exp\left[-\frac{z_v e\zeta}{k_B T}\frac{\cosh(\kappa y)}{\cosh(K)}\right] \tag{11}$$

where $\mu_{ep}^* = \mu_{ep}\big/z_v = De\big/k_B T$ can be viewed as the unit electrophoretic mobility, and $K = \kappa w$ is the nondimensional electrokinetic width. In EOF, the pressure drop P vanishes. In pressure-driven flow, however, the electric field E is simply replaced by the induced streaming potential field E_{st} given by (see the Addendum for the derivation)

$$E_{st} = -\frac{\mu_{eo}[1 - \tanh(K)/K]}{\mu_{eo}^2 K\left[\tanh(K) - K/\cosh^2(K)\right]\big/4\mu_{pd} + \sigma F_3}P \tag{12}$$

$$F_3 = \int_0^w \cosh\left[\frac{z_v e\zeta}{k_B T}\frac{\cosh(\kappa y)}{\cosh(K)}\right]d\left(\frac{y}{w}\right) \tag{13}$$

where σ is the bulk conductivity of the BGE. It is noted that the function F_3 defined in Eq. (13) is reflective of the surface conductance (see the Addendum), which could be significant in nanofluidic channels.

2.3 Solute separation in nanofluidic channels

The explicit inclusion of solute valence z_v in all the three velocity components of U_s in Eq. (10) indicates a potential separation of solutes, based on z_v, in both pressure- and electric field-driven flows. Those solutes differing solely in $\mu_{ep}^* = De/k_B T$ (virtually the diffusivity D) can only be electrophoretically separated, which is, however, still available in both types of flows because of the presence of the electric field therein (either externally applied in electric field-driven flow or internally induced in pressure-driven flow). In order to compare fairly the efficiency of solute separation in between the two flow patterns, we define the ratio of mean migration velocity between charged and neutral solutes, that is

$$\frac{U_s}{U_{neutral}} = \frac{U_s}{\frac{2}{3}\mu_{pd}P + \mu_{eo}E[1 - \tanh(K)/K]} \tag{14}$$

Therefore, the deviation of $U_s/U_{neutral}$ from unity indicates the separation of a charged solute from a neutral solute, and the difference in $U_s/U_{neutral}$ indicates the separation between two charged solutes because $U_{neutral}$ has nothing to do with the solute properties. Moreover, the ratio $U_s/U_{neutral}$ is independent of the driving force (E or P) because the pressure drop P vanishes in EOF while the induced electric field E is proportional to P in pressure-driven flow (see Eq. 12).

In typical microfluidic channels with $K >> 1$, it is easy to obtain from Eqs. (10), (11), and (14) the following ratio,

$$\left.\frac{U_s}{U_{neutral}}\right|_{K\to\infty} = \frac{\frac{2}{3}\mu_{pd}P + \mu_{eo}(1 + z_v\gamma)E}{\frac{2}{3}\mu_{pd}P + \mu_{eo}E} \tag{15}$$

where $\gamma = \mu_{ep}^*\big/\mu_{eo} = -De\eta/\varepsilon\zeta k_B T$ is the mobility ratio between solute electrophoresis and liquid electroosmosis and is positive in negatively charged channels. Therefore, solutes differing in z_v and/or γ cannot be effectively separated in pressure-driven flow through a microchannel because the EDL is so thin that the induced streaming potential field, Eq. (12), is negligible [17, 19], *i.e.*, $U_s|_{K\to\infty} \cong U_{neutral} = 2\mu_{pd}P/3$. In nanofluidic channels, however, the EDL thickness is comparable to the channel width such that on one hand, the streaming potential field or the so-called electro-viscous effect gets strong [6–9, 17], and on the other, the solute–wall interactions significantly affect the migration velocity of charged solutes, regardless of the flow pattern of the BGE [16]. Therefore, solutes in nanofluidic channels can be separated in both pressure- and electric field-driven flows.

In order for a straightforward understanding of the solute separation in nanofluidic channels, we propose a simplification to the mean migration velocity of solutes U_s in Eq. (10). Assuming a very small ζ such that $\zeta^* = e\zeta/k_B T << 1$ yields $G(\gamma) \approx 1 - z_v\zeta^*\cosh(\kappa\gamma)/\cosh(\kappa w)$ (see Eq. 11) and $F \approx 1$ (see Eq. 13), and hence reduces Eq. (10) to

$$U_{s\_simp} = \mu_{pd}P\left\{1 - \frac{K/3 - z_v\zeta^*\left[\tanh(K) - 2/K + 2\tanh(K)/K^2\right]}{K - z_v\zeta^*\tanh(K)}\right\} + \mu_{eo}E\left\{1 - \frac{\tanh(K) - z_v\zeta^*\left[\tanh(K) + K/\cosh^2(K)\right]/2}{K - z_v\zeta^*\tanh(K)}\right\} + z_v\mu_{ep}^* E \tag{16}$$

Compared to those of neutral solutes (*i.e.*, the denominator of the right-hand side of Eq. 14), both the pressure-driven and the electroosmotic velocity components in Eq. (16) are enhanced for negatively charged solutes ($z_v\zeta^* > 0$) but

reduced for positively charged solutes ($z_v\zeta^*<0$) wherein a negative zeta potential has been assumed.

There is, however, a distinct difference in the influence of solute electrophoretic motion between pressure- and electric field-driven flows. For example, consider the case $z_v\zeta^*<0$, *i.e.*, positively charged solutes ($z_v>0$) transported in a nanochannel carrying negative surface charge ($\zeta^*<0$)[1]. The three mobilities μ_{pd}, μ_{eo}, and μ^*_{ep} in Eq. (16) are now all positive. In electric field-driven flows ($P = 0$), the positive electroosmotic velocity component is decreased with the rise of z_v, while, at the same time, the positive electrophoretic velocity component is increased. Therefore, the variation of mean migration velocity U_{s_simp} with respect to z_v is mitigated. Similarly, in pressure-driven flows the positive pressure-driven velocity component gets smaller for solutes with a larger z_v. From Eq. (12), we know that the induced streaming potential field E_{st} points to the opposite direction of the applied pressure drop P. Therefore, the enhanced solute electrophoretic motion, which is against the pressure-driven flow, should improve the solute separation differing in z_v. However, the smaller magnitude of the induced electroosmotic backflow at a larger z_v tends to hinder the solute separation. The real efficiency of solute separation in electric field-driven and pressure-driven nanochannel flows will be discussed in the proceeding section.

3 Results and discussion

In this section, we compare the efficiency of solute separation in pressure- and electric field-driven nanochannel flows in terms of the ratio of mean migration velocity $U_s/U_{neutral}$ defined in Eq. (14). The two main factors affecting the separation efficiency, *i.e.*, solute valence z_v and mobility ratio γ (virtually the solute diffusivity D), will be examined individually in channels of different electrokinetic width K (or half-width w). We also demonstrate the improved separation efficiency of solutes transported in a combined pressure- and electric field-driven flow. The physicochemical properties [27] used in the calculations are summarized in Table 1 or otherwise noted in the figure captions.

Figure 2 shows the comparison of $U_s/U_{neutral}$ for charged solutes with valences $z_v = \pm2$ and ±1 between (a) pressure- and (b) electric field-driven nanochannel flows where the mobility ratio is fixed at $\gamma = 0.055$ (or the solute diffusivity $D = 5\times10^{-11}$ m^2/s). We see in pressure-driven flow negatively charged solutes always move faster than neutral ones while positively charged solutes move slower. Such velocity differences due to the solute–wall interactions become more significant when the electrokinetic width K shrinks, indicating higher separation efficiency in narrower nanochannels. Specifically, all $U_s/U_{neutral}$ curves in Fig. 2a achieve their extremes at around $K = 4$ corresponding to a half-channel width $w = 40$ nm, where the induced streaming potential field is believed to approach its maximum [17, 19]. In electric field-driven flow, however, there appear crossovers in $U_s/U_{neutral}$ curves, which necessitate a cautious identification of solutes in nanochannels of different widths. This phenomenon is attributed to the competitive effect between electroosmosis and electrophoresis as noted above. Moreover, the $U_s/U_{neutral}$ curves in electric field-driven flow are more closely gathered compared to those in pressure-driven flow. Therefore, solutes differing merely in valence are more efficiently separated in pressure-driven nanochannel flows. In addition, we notice that all $U_s/U_{neutral}$ curves in Fig. 2b achieve their extremes within almost the same range of K as in Fig. 2a, indicating the most desirable width of nanochannels for solute separation. As an example, Fig. 2c demonstrates the transport of an initially 1 μm wide solute zone 5 s after a vacuum of −60 kPa was imposed to the outlet of a 600 μm long, 100 nm wide channel. The attraction of positively charged solutes into the EDL where the wall viscous retardation is effective explains why they move slower than negatively charged solutes that are focused to the channel center where the fluid moves the fastest [11–16].

Figure 3 compares the ratio $U_s/U_{neutral}$ for monovalent negative solutes with variable mobility ratios γ (note: $\gamma_0 = 0.055$) between (a) pressure- and (b) electric field-driven nanochannel flows. For these solutes, the velocity component(s) associated with the fluid motion, *i.e.*, the pressure-driven and/or the electroosmotic velocity component in the mean migration velocity U_s, remains constant. In other words, only the difference in electrophoretic velocity component contributes to the solute separation. As the streaming effect is just a secondary effect in pressure-driven flow, solutes differing in γ are basically hard to separate, especially when the magnitude of γ is small. In electric field-driven

Table 1. Summary of physicochemical properties used in the calculations unless otherwise noted in the figure captions

	Properties	Values
BGE	Permittivity ε	7.08×10^{-10} CV^{-1}m^{-1}
	Viscosity ζ	1×10^{-3} kg·m^{-1}s^{-1}
	Ionic density n_0	6.022×10^{23} m^{-3}[a)]
	Temperature T	298 K
Nanofluidic channels	Length	600 μm
	Zeta potential ζ	–50 mV
Dissolved solutes	Diffusion coefficient D	5×10^{-11} m^2/s
	Mobility ratio γ	0.055
	Bulk concentration c_0	10 μM
	Half width of initial solute band w_0	0.5 μm
	Center of initial solute band X_0	10 μm

a) Note: This ionic density corresponds to the ionic concentration of 1 mM.

[1] This analysis also applies to negatively charged solutes transported in a nanochannel carrying positive surface charge where $z_v\zeta^*<0$ also holds.

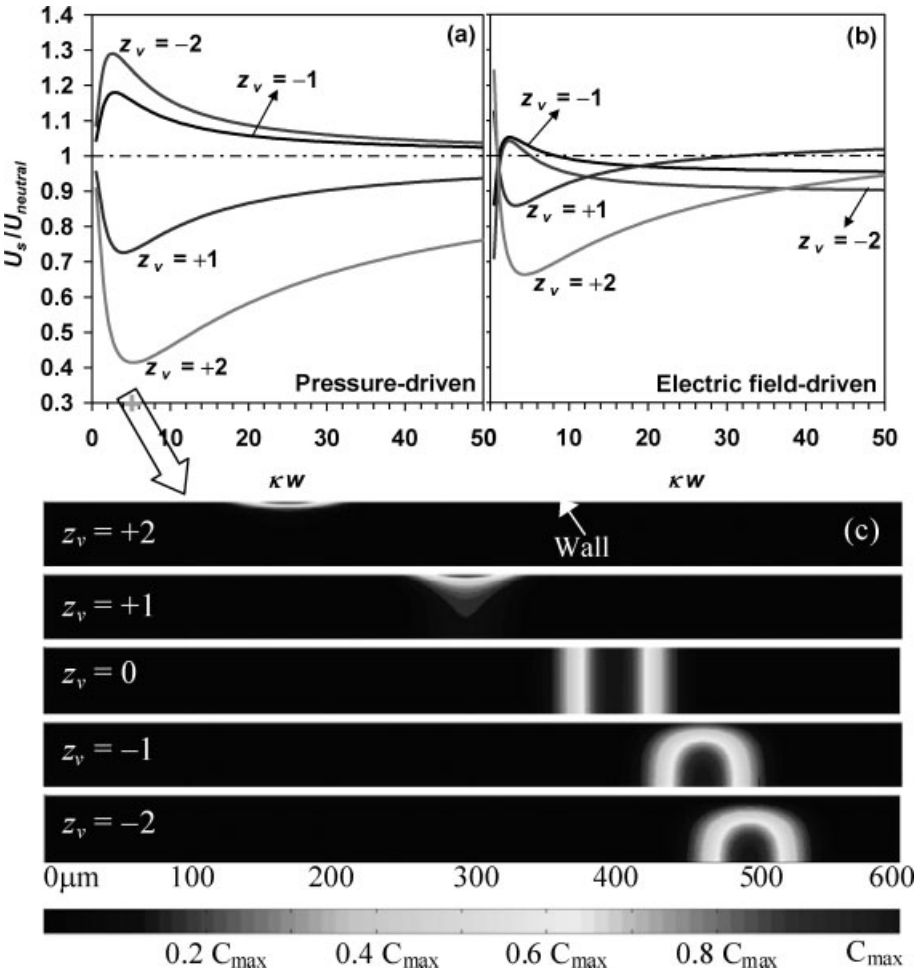

Figure 2. Comparison of the ratio of the mean migration velocity $U_s/U_{neutral}$ for solutes with different valences z_v transported in between (a) pressure- and (b) electric field-driven nanochannel flows. (c) Pressure-driven solute transport in a 100 nm wide channel at $t = 5$ s (only top half-channel is illustrated). The hollow arrow pointing to (c) indicates the equivalent nondimensional electrokinetic width K (noted by a cross in the abscissa of (a)) in (c). In all cases, a uniform solute band of half-width $w_0 = 0.5$ μm and concentration $c_0 = 10$ μM was initially injected to the same position $X_0 = 10$ μm downstream from the channel inlet. The applied pressure drop *per* unit channel length is $P = 1 \times 10^8$ Pam^{-1}. For all other parameters refer to Table 1. Differently shaded maps are used for the cases demonstrated, where, however, C_{max} always indicates the maximum concentration in each case.

flow, however, such solutes can be easily distinguished due to their dramatic difference in electrophoretic velocity. Figure 3c compares the transport of an initially 1 μm wide solute zone 5 s after an axial electric field of $E = 3$ kV/m is applied across a negatively charged nanochannel of width 100 nm. The higher the mobility ratio is, the slower the solute moves due to the larger negative electrophoretic velocity. Moreover, the solute with a higher mobility ratio is more significantly dispersed due to the greater diffusion coefficient.

It is now clear that in nanofluidic channels, pressure-driven flow can separate efficiently solutes with different valences z_v, while separate trivially those differing only in mobility ratio γ. Electric field-driven flow in nanochannels does the opposite thing. Naturally, we turn to the combination of these two types of flows. Figure 4 demonstrates the improved $U_s/U_{neutral}$ in pressure-driven nanochannel flow where an electric field of $E = \beta E_{st}$ is applied to generate an electroosmotic backflow. Note that $\beta = 1$ corresponds exactly to the pressure-driven flow we analyzed earlier. At a higher magnitude of β, all the $U_s/U_{neutral}$ curves illustrated in Fig. 4 go further away from the reference line $U_s/U_{neutral} = 1$ (*i.e.*, the ratio for neutral solutes). Therefore, the separation efficiency of solutes varying in either solely valence or solely mobility ratio is enhanced when the electroosmotic backflow grows stronger. However, it is also apparent that the separation of solute with $z_v = +1$ and $\gamma = 5\gamma_0$ from the one with $z_v = +2$ and $\gamma = \gamma_0$ is degraded with the increase of β. In such a case, we may reverse the EOF to improve the separation. Anyway, such a method of combining pressure- and electric field-driven flows should be used with care for solute separation in nanofluidic channels.

4 Concluding remarks

We have demonstrated theoretically that the solute–wall interactions in nanofluidic channels enable the separation of solutes in both pressure- and electric field-driven flows. However, their separation efficiencies may be significantly different depending on the two characteristic properties of solutes, *i.e.*, valence and mobility ratio (equivalent to the solute diffusivity as noted in the text). Specifically, solutes differing in valence can be efficiently separated in pressure-driven flow while those with different mobility ratios have to

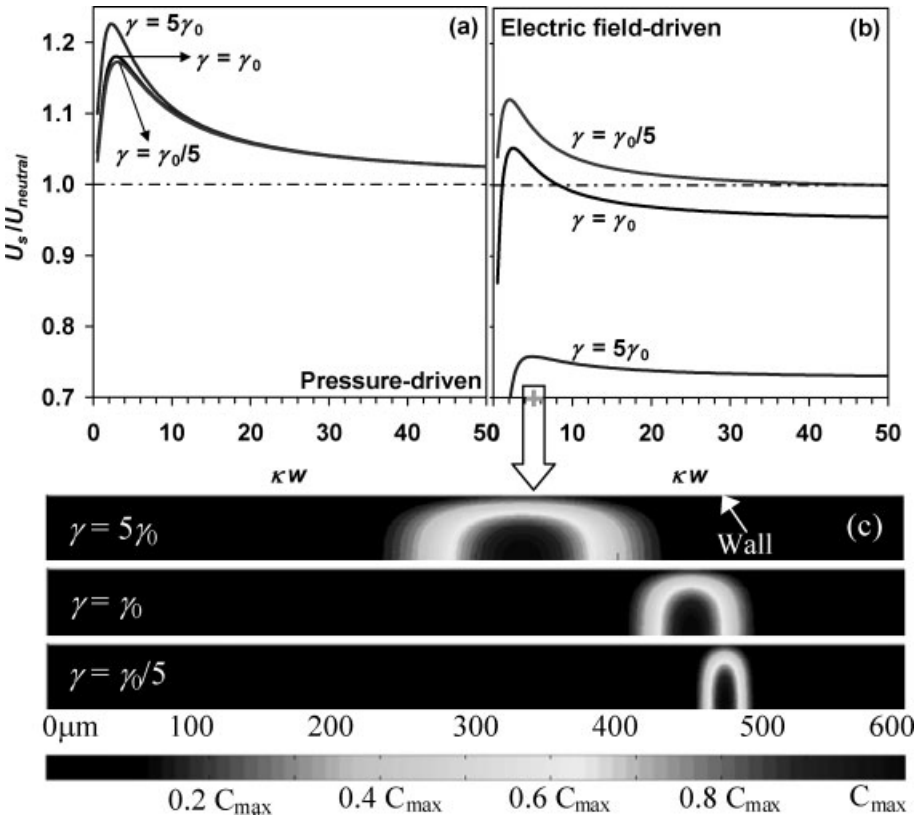

Figure 3. Comparison of the ratio of mean migration velocity $U_s/U_{neutral}$ for solutes with different mobility ratios γ transported in between (a) pressure- and (b) electric field-driven nanochannel flows. (c) Electric field-driven solute transport in a 100 nm wide channel at $t = 5$ s (only top half-channel is illustrated). The hollow arrow pointing to (c) indicates the equivalent non-dimensional electrokinetic width K (noted by a cross in the abscissa of (b)) in (c). The applied electric field is fixed as $E = 3$ kV/m. The reference mobility ratio is $\gamma_0 = 0.055$. For all other parameters refer to Fig. 2. Differently shaded maps are used for the cases demonstrated, where, however, C_{max} always indicates the maximum concentration in each case.

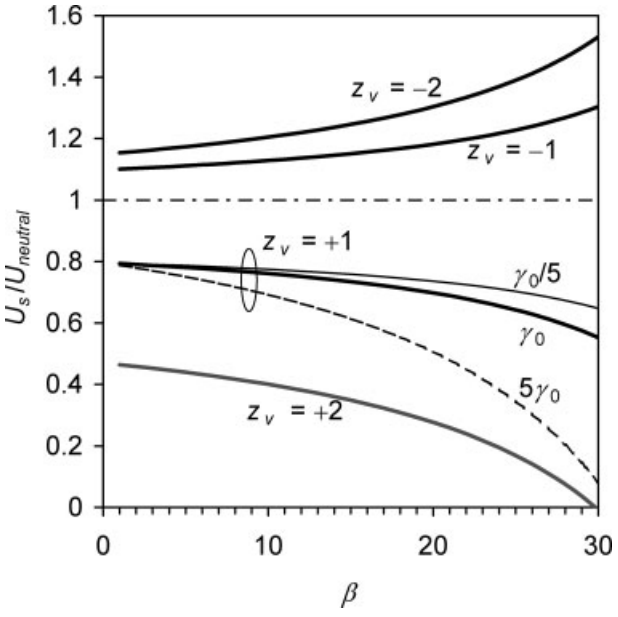

Figure 4. Ratio of mean migration velocity $U_s/U_{neutral}$ for solutes transported in a combined pressure- and electric field-driven flow. An electric field of $E = \beta E_{st}$ is applied to generate the electroosmotic backflow, where E_{st} is the induced streaming potential field. The ellipse groups the curves for monovalent negative solutes with variable mobility ratios γ, while all other curves share the same mobility ratio $\gamma_0 = 0.055$.

be separated in electric field-driven flow. We have also proposed a combined pressure- and electric field-driven flow in nanochannels for a better separation. In such a combined nanochannel flow, the separation efficiency of solutes varying in either valence or diffusivity alone is predicted to increase with increase in the magnitude of the electroosmotic backflow. However, this method may degrade the separation efficiency for solutes differing in both valence and diffusivity and thus should be used carefully.

Financial support from the Natural Sciences and Engineering Research Council (NSERC) of Canada, through a research grant to D. Li is gratefully acknowledged.

5 References

[1] Foret, F., Křivánková, L., Boček, P., *Capillary Zone Electrophoresis*, VCH Publishers Inc., New York 1993.

[2] Ardrey, R. E., *Liquid Chromatography-Mass Spectrometry: An Introduction*, John Wiley & Sons Ltd., England 2003.

[3] Eijkel, J. C. T., van den Berg, A., *Microfluid. Nanofluid.* 2005, *1*, 249–267.

[4] Mijatovic, D., Eijkel, J. C. T., van den Berg, A., *Lab Chip* 2005, *5*, 492–500.

[5] Chen, Y., Pepin, A., *Electrophoresis* 2001, *22*, 187–207.

[6] Stein, D., Kruithof, M., Dekker, C., *Phys. Rev. Lett.* 2004, *93*, 035901.

[7] Karnik, R., Fan, R., Yue, M., Li, D. *et al.*, *Nano Lett.* 2005, *5*, 943–8.

[8] Fan, R., Yue, M., Karnik, R., Majumdar, A., Yang, P. *et al.*, *Phys. Rev. Lett.* 2005, *95*, 086607.

[9] Van der Heyden, F. H. J., Stein, D., Dekker, C., *Phys. Rev. Lett.* 2005, *95*, 116104.

[10] Tseng, A. A., *Small* 2005, *1*, 594–608.

[11] Garcia, A. L., Ista, L. K., Petsev, D. N. *et al.*, *Lab Chip* 2005, *5*, 1271–6.

[12] Pennathur, S., Santiago, J. G., *Anal. Chem.* 2005, *77*, 6772–6781.

[13] Pennathur, S., Santiago, J. G., *Anal. Chem.* 2005, *77*, 6782–6789.

[14] Pennathur, S., Santiago, J. G., *Anal. Chem.* 2006, *78*, 972–972.

[15] Pennathur, S., Santiago, J. G., *Anal. Chem.* 2006, *78*, 972–973.

[16] Xuan, X., Li, D., *Electrophoresis* 2006, *27*, 5020–5031.

[17] Li, D., *Electrokinetics in Microfluidics*, Elsevier Academic Press, Oxford 2004.

[18] Lyklemma, J. K., *Fundamentals of Interface and Colloid Science*, Academic Press, New York 1995.

[19] Hunter, R. J., *Zeta Potential in Colloid Science: Principles and Applications*, Academic Press, New York 1981.

[20] Ajdari, A., Bontoux, N., Stone, H. A., *Anal. Chem.* 2006, *78*, 387–92.

[21] Jorgenson, J. W., Lukacs, K. D., *Anal. Chem.* 1981, *53*, 1298–302.

[22] Taylor, G., *Proc. R. Soc. Lond. A* 1953, *219*, 186–203.

[23] Aris, R., *Proc. R. Soc. Lond. A* 1956, *235*, 67–77.

[24] Griffiths, S. K., Nilson, R. H., *Anal. Chem.* 1999, *71*, 5522–9.

[25] Xuan, X., Li, D., *J. Micromech. Microeng.* 2004, *14*, 1171–1180.

[26] Carslaw, H. S., Jaeger, J. C., *Conduction of Heat in Solids*, 2nd Edn., Clarendon Press, Oxford 1959.

[27] Probstein, R. F., *Physicochemical Hydrodynamics*, 2nd Edn., John Wiley and Sons, New York 1994.

[28] Burgreen, D, Nakache, F. R., *J. Phys. Chem.* 1964, *68*, 1084–91.

[29] Hildreth, D., *J. Phys. Chem.* 1970, *74*, 2006–15.

[30] Xuan, X., Li, D., *J. Micromech. Microeng.* 2004, *14*, 290–8.

6 Addendum

6.1 Notation

c	solute concentration
c_0	initial solute concentration
c_c	solute concentration at the channel axis
D	diffusion coefficient
e	charge of a proton, 1.602×10^{-19} C
E	axial electric field
E_{st}	streaming potential field in pressure-driven flow
F/G	defined functions
k_B	Boltzmann's constant, 1.381×10^{-23} J K^{-1}
K	nondimensional electrokinetic width
n_0	bulk ionic density of BGE
P	pressure drop *per* unit channel length
t	time coordinate
T	temperature, 298 K (T_0 for ambient)
u	velocity of BGE in the longitudinal direction
U_s	mean migration velocity of solutes
$U_{neutral}$	mean migration velocity of neutral solutes
U_{s_simp}	simplified solution of U_s
w	half-channel width
w_0	half-width of the injected solute zone
x	streamwise or longitudinal coordinate
X_0	the central location of the injected solute zone
y	transverse coordinate
z_v	valence of solute ions
ε	permittivity
η	dynamic viscosity
γ	mobility ratio between electrophoresis and electroosmosis
κ	reciprocal of Debye length
μ	mobility
μ_{ep}^*	unit electrophoretic mobility
ψ	EDL potential
ψ_c	double layer potential at the channel axis
σ	electrical conductivity of the BGE
ζ	zeta potential, -50 mV
ζ^*	normalized zeta potential, $= e\zeta/k_BT$

Subscripts:

eo	electroosmotic
ep	electrophoretic
pd	pressure-driven

6.2 Electrokinetic flow field in a slit nanochannel

This Addendum presents the derivations of the EDL field, Eq. (8), flow field, Eq. (9), and streaming potential field, Eq. (12), in electrokinetic flow through a slit nanochannel; see Fig. 1 for the schematic. At steady-state, the Navier–Stokes equation is reduced to [28, 29]

$$\eta \frac{d^2u}{dy^2} + P + \rho_e E = 0 \tag{A1}$$

where P is the pressure drop *per* unit channel length, E is the axial electric field strength, and ρ_e is the net charge density given by the Poisson equation [18, 19]

$$\rho_e = -\varepsilon \frac{d^2\psi}{dy^2} \tag{A2}$$

Considering the no-slip boundary condition for Eq. (A1) and the Dirichlet boundary condition (*i.e.*, zeta potential) for Eq. (A2) on the channel wall ($y = w$), it is straightforward to obtain

$$u = \mu_{pd}\left(1 - \frac{y^2}{w^2}\right)P + \mu_{eo}\left(1 - \frac{\psi}{\zeta}\right)E \tag{9}$$

where the definitions of μ_{pd} and μ_{eo} are the same as mentioned previously. It is noted that in the net charge density, ρ_e in Eq. (A2), we have neglected the contribution from the charged solutes in order to simplify the analysis. This neglect is reasonable as long as the solute concentration is much lower than the ionic concentration of the BGE, which is fulfilled in typical electrophoretic separations. Under such a condition, it is also safe to assume a uniform zeta potential on the channel wall. The EDL potential ψ is determined from the Poisson–Boltzmann equation that can be simplified to Eq. (A3) under the Debye–Hückel approximation [17–19]

$$\frac{d^2\psi}{dy^2} = \kappa^2\psi \tag{A3}$$

where $\kappa = \sqrt{2e^2 n_0/\varepsilon k_B T}$ is the inverse of Debye length. Note that we have assumed here a symmetric electrolyte solution with unit charge, for example, KCl, for simplicity. Hence, the EDL potential field is easily solved as

$$\psi = \zeta\frac{\cosh(\kappa y)}{\cosh(\kappa w)} \tag{8}$$

Assuming equal ionic mobilities for the positive and negative ions of the electrolyte, the electrical current density is given by [17, 29, 30]

$$j = \rho_e u + \sigma\cosh\left(\frac{z_v e\psi}{k_B T}\right)E \tag{A4}$$

where σ is the bulk conductivity of the electrolyte. It is important to note that the cosh term in Eq. (A4) accounts for the distribution of the real conductivity across the channel due to the effect of the so-called surface conductance [17–19]. Substituting Eqs. (8) and (9) into Eq. (A4) and then integrating it over a unit channel cross-section yields the average current density J in electrokinetic flow

$$J = \mu_{eo}F_1 P + \left(\frac{\mu_{eo}^2}{\mu_{pd}}F_2 + \sigma F_3\right)E \tag{A5}$$

$$F_1 = 1 - \tanh(K)/K \tag{A6}$$

$$F_2 = K\left[\tanh(K) - K/\cosh^2(K)\right]/4 \tag{A7}$$

$$F_3 = \int_0^w \cosh\left[\frac{z_v e\zeta}{k_B T}\frac{\cosh(\kappa y)}{\cosh(K)}\right]d\left(\frac{y}{w}\right) \tag{13}$$

For a steady-state pressure-driven flow, there is no net current in the channel, *i.e.*, $J = 0$. As such, a streaming potential field E_{st} is produced by the applied pressure drop

$$E_{st} = -\frac{\mu_{eo}F_1}{\mu_{eo}^2 F_2\Big/\mu_{pd} + \sigma F_3}P \tag{A8}$$

Recovering the functions F_1 and F_2 then gives Eq. (12) in the main text.

